DOI: 10.1002/chem.200500171

Solid- and Solution-State Studies of the Novel μ-Dicyanamide-Bridged Dinuclear Spin-Crossover System $\{[(Fe(bztpen)]_2[\mu\text{-}N(CN)_2]\}(PF_6)_3 \cdot n H_2O$**

Norma Ortega-Villar,[a, d] Amber L. Thompson,[b] M. Carmen Muñoz,[c] Víctor M. Ugalde-Saldívar,[d] Andrés E. Goeta,[b] Rafael Moreno-Esparza,*[d] and José A. Real*[a]

Abstract: The mononuclear diamagnetic compound $\{Fe(bztpen)[N(CN)_2]\}(PF_6)CH_3OH$ (**1**) (bztpen = *N*-benzyl-*N*,*N*′,*N*′-tris(2-pyridylmethyl)ethylenediamine) has been synthesized and its crystal structure studied. Complex **1** can be considered to be the formal precursor of two new dinuclear, dicyanamide-bridged iron(II) complexes with the generic formula $\{[(Fe(bztpen)]_2[\mu\text{-}N(CN)_2]\}(PF_6)_3 \cdot n H_2O$ (n = 1 (**2**) or 0 (**3**)), which have been characterized in the solid state and in solution. In all three complexes, the iron atoms have a distorted $[FeN_6]$ octahedral coordination defined by a bztpen ligand and a terminal (**1**) or a bridging dicyanamide ligand (**2** and **3**). In the solid state, **2** and **3** can be considered to be molecular isomers that differ by the relative position of the phenyl ring of the two $\{Fe(bztpen)[N(CN)_2]\}^+$ halves (*cis* and *trans*, respectively). Depending on the texture of the sample, **2** exhibits paramagnetic behavior or displays a very incomplete spin transition at atmospheric pressure. Complex **3** undergoes a gradual two-step spin transition with no observed hysteresis in the solid state. Both steps are approximately 100 K wide, centered at ≈200 K and ≈350 K, with a plateau of approximately 80 K separating the transitions. The crystal structure of **3** has been determined in steps of approximately 50 K between 400 K and 90 K, which provides a fascinating insight into the structural behavior of the complex and the nature of the spin transition. Order–disorder transitions occur in the dicyanamide bridge and the PF_6^- ions simultaneously, with the spin-crossover behavior suggesting that these transitions may trigger the two-step character. In solution, **2** and **3** display very similar continuous spin conversions. Electrochemical studies of **2** and **3** show that the voltammograms are typical of dimeric systems with electronic coupling of the metals through the dicyanamide ligand.

Keywords: dinuclear compounds · iron complexes · spin crossover · X-ray diffraction

Introduction

In recent years, considerable effort has been focused on the synthesis of molecular materials exhibiting physical properties that may be switched in a controlled manner because they are potentially good candidates for signal generation and processing. This is particularly true within the realm of spin crossover (SCO) and related cooperative phenomena, where interesting examples of thermal, pressure, light and magnetic-field switching between two states have been provided.[1] In addition, it was realized long ago that the possible coexistence of SCO and magnetic coupling in polynuclear compounds could be exploited to modulate a magnetic signal.[2] It was foreseen that the nature of intramolecular ferromagnetic or antiferromagnetic coupling in such systems could be modified to switch the spin state of the SCO units. Nowadays, only a few examples can be found showing this phenomenology in which magnetic exchange and SCO coexist in the same material.[3] The interplay between intramolecular antiferromagnetic interactions and SCO has been ex-

[a] N. Ortega-Villar, Prof. Dr. J. A. Real
Institut de Ciencia Molecular/Departament de Química Inorgánica
Universitat de València
Doctor Moliner 50, 46100 Burjassot (Spain)
Fax: (+34) 963-544-859
E-mail: jose.a.real@uv.es

[b] Dr. A. L. Thompson, Dr. A. E. Goeta
Department of Chemistry, University of Durham
South Road, Durham DH1 3 LE (UK)

[c] Prof. Dr. M. C. Muñoz
Departament de Física Aplicada, Universitat Politècnica de València
Camino de Vera s/n, 46071, Valencia (Spain)

[d] N. Ortega-Villar, Prof. Dr. V. M. Ugalde-Saldívar,
Prof. Dr. R. Moreno-Esparza
Facultad de Química (UNAM)
Edificio B. Av. Universidad 3000, Coyoacán, Mexico D.F. 04510 (México)
Fax: (+52) 555-616-2010
E-mail: moresp@servidor.unam.mx

[**] bztpen = *N*-benzyl-*N*,*N*′,*N*′-tris(2-pyridylmethyl)ethylenediamine.

Supporting information for this article is available on the WWW under http://www.chemeurj.org/ or from the author.

hibited in some {[Fe(L)(NCX)$_2$]$_2$(μ-bpym)} compounds, notably those with L = bpm, X = S or Se ([bpm, S] and [bpm, Se]) and L = 2,2′-bithiazoline (bt), X = S ([bt, S]). Studies have been carried out by perturbing the system by changing the temperature and/or pressure and with light irradiation (LIESST effect). These experiments have made it possible to identify the occurrence of different kinds of spin-pair states in these compounds, namely LS–LS, LS–HS, and HS–HS in which, for instance, LS–HS indicates that, in a dinuclear unit, one iron(II) atom is low-spin (LS), while the other is high-spin (HS). A singular feature in these compounds is the occurrence of a plateau between two separate spin transitions that each involve ≈50% of the iron ions. This plateau has been associated with the existence of the mixed spin state LS–HS. Unfortunately, standard single-crystal X-ray studies carried out on compound [bt, S] in the middle of the plateau have not enabled the observation of the predicted symmetry change in crystals that involve the transformations HS–HS⇄LS–HS and LS–LS⇄LS–HS.[3h,i] However, this hypothesis has found new support in the novel dinuclear compound {[Fe(phdia)(NCS)$_2$]$_2$(μ-phdia)}.[4] Recent contributions from Brooker, Murray, and Kaizaki and co-workers have reported new iron(II) dinuclear SCO compounds that have added new interesting results in this field,[5–7] further details of which are given later. It is also worth mentioning that two-step transitions are not a singularity associated exclusively with the dinuclear nature of the system as there are a few well-characterized mononuclear and polymeric compounds exhibiting two-step SCO. In this respect, long-range ordering interactions inducing spontaneous symmetry breaking and formation of an intermediate phase in which HS and LS molecules coexist at a 1:1 ratio has been observed for {[Fe(pic)$_3$]Cl$_2$·EtOH}[8] (where pic = 2-picolylamine). Furthermore, this behavior is also observed in [Fe(btzb)$_3$](PF$_6$)$_2$, where btzb = tris(1,4-bis(tetrazol-1-yl)-butane-*N*4, *N*4′).[8b] Similarly, the occurrence of infinite chains of alternate ···LS–HS-LS··· states has been observed in the plateau displayed by the three-dimensional polymer {Fe(pmd)[Ag(CN)$_2$][Ag$_2$(CN)$_3$]},[9a] and the presence of interlayer elastic interactions in the 2D polymer [Fe(H$_3$L^{Me})]-[Fe(L^{Me})]X (where L^{Me} = tris[2-{[(2-methylimidazol-4-yl)-methylidene]amino}ethyl]amine and X = ClO$_4^-$, BF$_4^-$, PF$_6^-$, and AsF$_6^-$) has been shown to produce a HS-LS state in the plateau.[9b]

Currently, the study of new dinuclear SCO compounds represents a challenge, not only with regard to the fundamental and synthetic aspects, but also because they represent the first step in the search for new functional polynuclear nanomaterials, an almost unexplored area of research in molecular chemistry. In this regard, the synthesis and characterization of the first tetranuclear iron(II) SCO compound has recently been reported.[10] In our pursuit of new polynuclear SCO compounds, we have explored an alternative synthetic approach based on the use of [Fe^{II}(L)(X)]$^{n+}$ moieties, where L is a pentadentate ligand and X is a labile solvent molecule or an anionic ligand susceptible to being substituted by a suitable bridge—which is dicyanamide in the complexes discussed in this paper. Toftlund, McKenzie, and co-workers adopted this strategy in similar pentadentate compounds from a bioinorganic perspective (see ref. [19]). Herein we report the synthesis, crystal structure, and magnetic characterization in the solid state of the LS precursor {Fe(bztpen)[N(CN)$_2$]}(PF$_6$)·CH$_3$OH (**1**) (bztpen = *N*-benzyl-*N*,*N*′,*N*′-tris(2-pyridylmethyl)ethylenediamine) and the related dinuclear system {[Fe(bztpen)]$_2$[N(CN)$_2$]}-(PF$_6$)$_3$·*n*S (S = solvent), which represents the first example of a μ-bridged dicyanamide dinuclear SCO complex. This

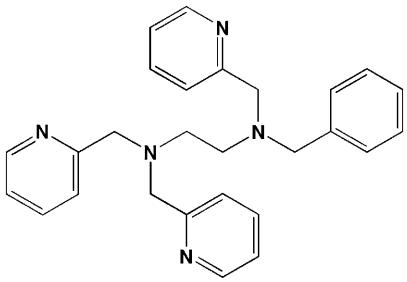

bztpen

compound undergoes a two-step spin transition whereas the occurrence and nature of the SCO in the corresponding monohydrate (**2**, which can be considered to be a coordination isomer of **3**), depends on the texture and history of the sample. Electrochemical, UV/Vis, and NMR (Evans method) studies have been also carried out in solution. The SCO behaviors have been analyzed within the framework of regular solution theory.[11]

Results

Solid-state magnetic properties: Compound **1** was found to be diamagnetic in the 400–4.2 K temperature region, indicating that the iron atom is in the LS ground state. Figure 1 shows the thermal dependence of the $\chi_M T$ product for **2** and **3** as a function of temperature, where χ_M is the molar magnetic susceptibility and T is the temperature. At 350 K, $\chi_M T$ is $\approx 6.7\ cm^3 K mol^{-1}$ for a sample of **2** (see Figure 1a, curve (1)) consisting of small single crystals (10.88 mg). This value is within the range of expected values for a complex consisting of two iron(II) ions in the HS state with a significant orbital contribution. $\chi_M T$ initially remains constant as the temperature is lowered, and below 50 K, it starts to decrease steeply to $3.17\ cm^3 K mol^{-1}$ at 4.2 K. This behavior may be attributed to the occurrence of zero-field splitting of the $S = 2$ ground state and/or a very weak intramolecular antiferromagnetic interaction mediated by the [N(CN)$_2$]$^-$ bridge between the iron atoms. Precipitated microcrystalline samples behave similarly to the single crystals; however, in general, the former undergoes a very incomplete and relatively steep spin transition at $T_c \approx 170$ K involving less than 20% of the iron atoms on warming from 4 K. The extent of the transition depends on the history of the sample. For example, after two cooling–warming cycles, the conversion de-

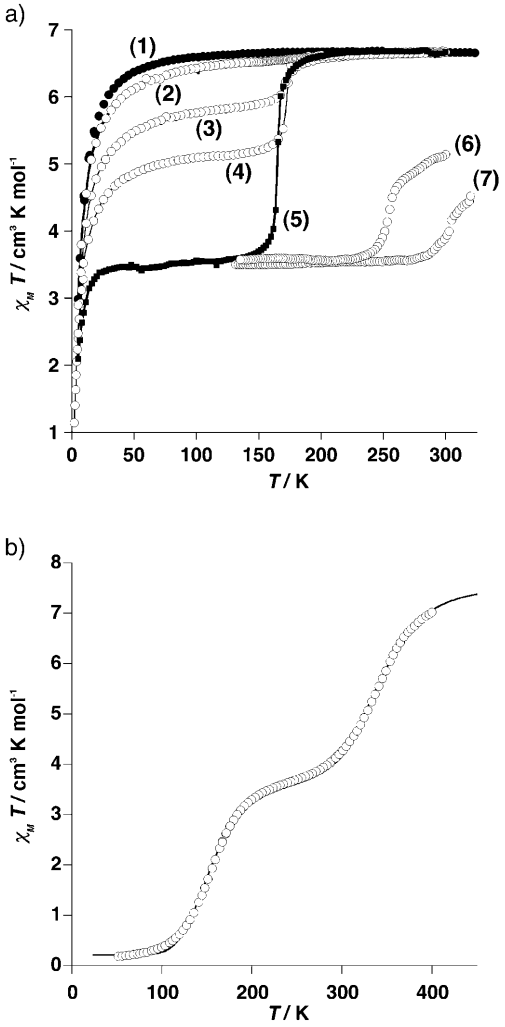

Figure 1. Magnetic properties in the solid state. a) $\chi_M T$ versus T plots for compound **2**: (1) single crystals; (2–4) precipitated sample after annealing; (5–7) measurements of the single crystals in the high-pressure cell at 1 bar, 3.2 kbar, and 6.4 kbar, respectively (see text). b) $\chi_M T$ versus T plots for compound **3**, the solid line represents the best fits between calculated and experimental data.

creases from ≈20% to 10% or even vanishes (Figure 1a, curves (4), (3), and (2), respectively), which is probably attributable to damage to the crystals. Interestingly, when freshly prepared single crystals (5.46 mg) are measured in a high-pressure cell at 1 bar, they display a cooperative transition, without hysteresis, involving 50% of the iron atoms at T_c = 165 K (Figure 1a, curve (5)). This could be the result of two combined effects: 1) a very small hydrostatic pressure generated by the silicone oil used for transmitting pressure in the cell, and 2) the fact that the sample is wetted by the oil. As the pressure is increased, T_c increases and the amount of HS species present at 300 K decreases (Figure 1a, curves (5)–(7)). At 6.4 kbar, compound **2** has essentially 50% of the iron(II) atoms in the LS state, at 300 K.

For compound **3** (Figure 1b, white circles), $\chi_M T$ = 7.0 cm^3 K mol^{-1} at 400 K, indicating that this complex is essentially in the HS state. However, as the temperature is lowered, $\chi_M T$ decreases continuously reaching a plateau in the temperature region ≈285–208 K. The average value of the plateau is $\chi_M T$ ≈3.65 cm^3 K mol^{-1} at 250 K. Below 210 K, $\chi_M T$ decreases again in a second step, and $\chi_M T$ = 0.21 cm^3 K mol^{-1} at 50 K. This behavior indicates the occurrence of an almost complete two-step $S = 2 \rightleftarrows S = 0$ spin conversion in the dinuclear species involving ≈50% of iron(II) atoms in each step (HS molar fraction γ_{HS} = 0.5). The characteristic temperature, at which the HS molar fraction of each step is γ_{HS_i} = 0.5 (i = 1, 2), is T_{c1} = 342.4 K, and T_{c2} = 156.8 K for the first and second steps, respectively. Owing to the lack of cooperativity, these conversions can be considered as two consecutive spin equilibriums supposedly taking place between the species HS–HS, LS–HS, and LS–LS according to Equation (1), where n_{HH}, n_{HL}, and n_{LL} are the number of moles of the species HS–HS, HS-LS, and LS–LS, respectively.

$$\underset{n_{HH}}{HS\text{—}HS} \overset{K_1}{\rightleftharpoons} \underset{n_{HL}}{LS\text{—}HS} \overset{K_2}{\rightleftharpoons} \underset{n_{LL}}{LS\text{—}LS} \tag{1}$$

The equilibrium constants are $K_1 = n_{HL}/n_{HH}$ and $K_2 = n_{LL}/n_{HL}$. The $\chi_M T$ product can be expressed by Equation (2), where $n_T = n_{HH} + n_{HL} + n_{LL}$ and $(\chi_M T)_{HH}$ and $(\chi_M T)_{LH}$ correspond to the $\chi_M T$ value associated to 100% of HS–HS and LS–HS species, respectively.

$$\chi_M T = \frac{n_{HH}}{n_T}(\chi_M T)_{HH} + \frac{n_{LH}}{n_T}(\chi_M T)_{LH} \tag{2}$$

The introduction of the equilibrium constants into Equation (2) gives Equation (3).

$$\chi_M T = \frac{K_1 K_2 (\chi_M T)_{HH} + K_2 (\chi_M T)_{LH}}{1 + K_1 K_2 + K_2} \tag{3}$$

Inclusion of the thermal dependence of the equilibrium constants gives Equation (4).

$$K_i(T) = \exp\left(-\frac{\Delta H_i}{RT} + \frac{\Delta S_i}{R}\right) = \exp\left[\frac{\Delta S_i}{R}\left(1-\frac{T_{ci}}{T}\right)\right] \tag{4}$$

Consequently, Equation (3) can be rewritten as a function of the characteristic T_{ci} temperature and ΔS_i to give Equation (5), where the term $(\chi_M T)_R$ has been added to account for residual paramagnetism at low temperature and $(\chi_M T)_{HL}$ is considered to be equal to $(\chi_M T)_{HH}/2$.

$$\chi_M T = \frac{(\chi_M T)_{HH} \cdot \exp\left[\frac{\Delta S_2}{R}\left(1-\frac{T_{c2}}{T}\right)\right] \cdot \exp\left[\frac{\Delta S_1}{R}\left(1-\frac{T_{c1}}{T}\right)\right] + (\chi_M T)_{LH} \cdot \exp\left[\frac{\Delta S_2}{R}\left(1-\frac{T_{c2}}{T}\right)\right]}{1 + \exp\left[\frac{\Delta S_2}{R}\left(1-\frac{T_{c2}}{T}\right)\right] \cdot \exp\left[\frac{\Delta S_1}{R}\left(1-\frac{T_{c1}}{T}\right)\right] + \exp\left[\frac{\Delta S_2}{R}\left(1-\frac{T_{c2}}{T}\right)\right]} + (\chi_M T)_R \tag{5}$$

The best least-squares fit of Equation (5) is in excellent agreement with the experimental measurements (see Figure 1b, solid line). The parameters obtained from the fit are $\Delta S_1 = 114\,J\,K^{-1}\,mol^{-1}$, $\Delta S_2 = 63.4\,J\,K^{-1}\,mol^{-1}$, $(\chi_M T)_{HH} = 7.26\,cm^3\,K\,mol^{-1}$, and $(\chi_M T)_R = 0.21\,cm^3\,K\,mol^{-1}$. For $T_{ci} = \Delta H_i/\Delta S_i$, the values for the enthalpy variations are $\Delta H_1 = 39\,kJ\,mol^{-1}$ and $\Delta H_2 = 9.9\,kJ\,mol^{-1}$. However, the thermodynamic parameters deduced for the first step actually correspond to the total transformation of the HS–HS species to the LS–LS species. Consequently, the correct parameters for the HS–HS→LS–HS transformation are in fact $\Delta S_1' = \Delta S_1/2 = 57\,J\,K^{-1}\,mol^{-1}$ and $\Delta H_1' = \Delta H_1/2 = 19.5\,kJ\,mol^{-1}$. These thermodynamic parameters agree quite well with what is expected for an almost complete $S = 2 \rightleftarrows S = 0$ spin conversion.

Crystal and molecular structure of 1: The molecular structure of **1** is displayed in Figure 2 together with the atom numbering scheme. Complex **1** crystallizes in the triclinic space group $P\bar{1}$. The iron atom is in a distorted octahedral [FeN_6] environment, whereby five of the nitrogen atoms belong to the pentadentate bztpen ligand and the remaining position is occupied by the dicyanamide anion, which acts as a monodentate ligand. A disordered PF_6^- group balances the charge of the {Fe(bztpen)[$N(CN)_2$]}$^+$ species and there is one additional methanol solvent molecule in the asymmetric unit. The bztpen ligand is wrapped around the iron atom defining a distorted square pyramid with the nitrogen atom N(5) lying on the axial apex. The N(5) atom is in the center of a tripod whose arms are defined by two picolylamine-like moieties (N(5)-C(16)-C(15)-N(1) and N(5)-C(26)-C(25)-N(2)) and one ethylenediamine-like moiety (N(5)-C(51)-C(52)-N(4)). These arms are anchored to the iron atom by the N(1), N(2), and N(4) atoms. The Fe–N bond lengths average 2.0 Å (Fe(1)–N(1) = 1.975(3), Fe(1)–N(2) = 1.963(3), and Fe(1)–N(4) = 2.086(3) Å), with a similar bond length to N(5). (2.002(3) Å) The fifth nitrogen atom of the square pyramid, N(3), belongs to a picolylamine-like fragment attached to the N(4) atom of the ethylene diamine-like moiety and the Fe(1)–N(3) bond length is 1.995(3) Å. The octahedron is completed by the N(6) atom belonging to the dicyanamide ligand (Fe(1)–N(6) = 1.955(4) Å), which is in a *trans* conformation with respect to N(5). These structural data indicate that the Fe atom is in the low-spin state at room temperature, in accordance with the magnetic measurements. The arrangement of the angles around the iron atom clearly shows distortion from the expected 90° and 180° for a regular octahedron. This is imposed by the geometrical constraints created by the structure of the ligand. In addition, the dicyanamide [$N(CN)_2$]$^-$ ion is bent (as would be expected, C(61)-N(7)-C(71) = 120.6(4)°) and while each N-C-N half has a different angle, they are almost linear (N(6)-C(61)-N(7) = 174.8(5) and N(8)-C(71)-N(7) = 172.9(6)°).

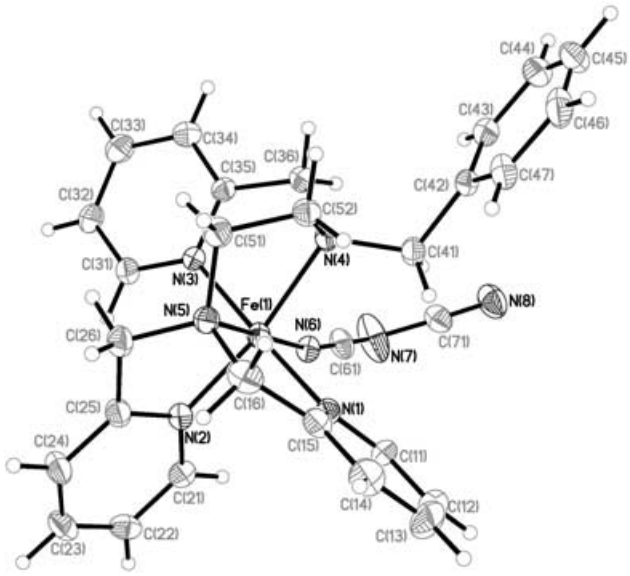

Figure 2. Molecular structure of compound **1** (displacement ellipsoids are shown at the 25% probability level for clarity).

No significant hydrogen bonding and/or π stacking is observed in the crystal, and cohesion appears to arise from the electrostatic interaction between {Fe(bztpen)[$N(CN)_2$]}$^+$ ions and PF_6^- ions. Relevant crystal data for **1** are presented in Table 1, selected bond lengths and angles are presented in Table 2.

Table 1. Crystallographic data for **1**, **2**, and **3**.

	1	**2**	**3**
formula	$C_{30}H_{33}F_6Fe_1N_8O_1P_1$	$C_{28}H_{30}F_9Fe_1N_{6.5}O_{0.5}P_{1.5}$	$C_{56}H_{58}F_{18}Fe_2N_{13}P_3$
M_w	722.46	738.89	1459.76
space group	$P\bar{1}$ (2)	$C2/c$ (15)	$P\bar{1}$ (2)
a[Å]	9.4229(3)	19.0640(4)	9.4161(7)
b[Å]	11.4330(4)	19.4420(6)	16.4923(13)
c[Å]	16.5440(8)	18.5770(4)	20.6515(15)
α[°]	81.312(2)	90	104.691(2)
β[°]	81.908(2)	104.0320(19)	90.747(2)
γ[°]	66.604(2)	90	97.624(2)
V[Å^3]	1610.43(11)	6680.0(3)	3071.1(4)
Z	2	8	2
T[K]	293(2)	293(2)	290(2)
λ[Å]	0.71073	0.71073	0.71073
μ[mm^{-1}]	0.592	0.605	0.656
ρ_{calcd}[g cm^{-3}]	1.490	1.469	1.579
$R1$[a]	0.0715	0.0699	0.0694
$wR2$	0.1436	0.1876	0.1181

[a] $R1 = \Sigma||F_o|-|F_c||/\Sigma|F_o|$; $wR2 = [\Sigma[w(F_o^2-F_c^2)^2]/\Sigma[w(F_o^2)^2]]^{1/2}$; $w = 1/[\sigma^2(F_o^2) + (mP)^2 + nP]$ where $P = (F_o^2 + 2F_c^2)/3$ (m = 0.0806 (**1**), 0.1470 (**2**), and 0.0526 (**3**); n = 0.0000 (**1**), 1.1304 (**2**), and 0.0000 (**3**)).

Table 2. Selected bond lengths [Å] and angles [°] for **1** and **2**.

	1	**2**
Fe–N(1)	1.975(3)	2.188(4)
Fe–N(2)	1.963(3)	2.148(4)
Fe–N(3)	1.995(3)	2.271(4)
Fe–N(4)	2.086(3)	2.224(4)
Fe–N(5)	2.002(3)	2.241(4)
Fe–N(6)	1.955(4)	2.065(4)
N(6)–C(61)	1.143(5)	1.130(7)
C(61)–N(7)	1.318(6)	1.292(7)
N(7)–C(71)	1.313(6)	
C(71)–N(8)	1.118(5)	
N(1)-Fe-N(2)	88.54(13)	100.06(15)
N(1)-Fe-N(3)	177.40(13)	172.63(15)
N(1)-Fe-N(4)	94.62(13)	98.24(15)
N(1)-Fe-N(5)	84.90(14)	76.28(15)
N(1)-Fe-N(6)	93.35(14)	92.33(18)
N(2)-Fe-N(3)	93.64(13)	85.33(14)
N(2)-Fe-N(4)	167.01(13)	145.44(14)
N(2)-Fe-N(5)	81.85(13)	75.07(15)
N(2)-Fe-N(6)	99.45(14)	102.96(17)
N(3)-Fe-N(4)	82.94(13)	74.61(14)
N(3)-Fe-N(5)	94.00(14)	100.49(14)
N(3)-Fe-N(6)	87.69(14)	91.34(17)
N(4)-Fe-N(5)	85.87(12)	81.18(14)
N(4)-Fe-N(6)	92.95(13)	105.31(16)
N(5)-Fe-N(6)	177.81(14)	167.74(16)
C(61)-N(6)-Fe	166.0(3)	166.3(5)
N(6)-C(61)-N(7)	174.8(5)	168.7(6)
C(71)-N(7)-C(61)	120.6(4)	
N(8)-C(71)-N(7)	172.9(6)	

Crystal and molecular structure of 2: Figure 3 shows the crystal structure of **2** together with the atom numbering scheme. Complex **2** crystallizes in the monoclinic space group *C*2/*c*. The compound is made up of a dinuclear cationic species $\{[(Fe(bztpen)]_2[N(CN)_2]\}^{3+}$ and three hexafluorophosphate (PF_6^-) anions together with one water molecule per formula unit. The cationic unit is made up of two identical $\{Fe(bztpen)\}^{2+}$ fragments, bridged by one $[N(CN)_2]^-$ ion. A twofold axis passing through the central nitrogen atom of the dicyanamide bridge N(7) relates the two halves of the dinuclear complex. The bztpen ligand surrounds the iron atom with Fe–N bond lengths Fe(1)–N(1-to-5) = 2.188(4), 2.148(4), 2.271(4), 2.224(4), and 2.241(4) Å, respectively, which are much longer than the Fe–N bond length to the dicyanamide unit Fe(1)–N(6) = 2.065(4) Å. The iron atom is in a severely distorted octahedral $[FeN_6]$ environment. The bond lengths and angles of the $[FeN_6]$ core differ considerably with respect to those of **1**. The bond lengths, much longer in **2**, are consistent with the HS state observed from the magnetic data. As in **1**, the geometrical constraints created by the structure of the bztpen ligand impose a departure from the octahedral arrangement of the Fe atom and the expected 90° and 180° for a regular octahedral system. In this respect, it is worthwhile noting that the absolute average difference of the bond angles from the regular octahedron is much bigger for **2** (9.96°) than for **1** (4.30°). In particular, the angles N(2)-Fe(1)-N(1), N(5)-Fe(1)-N(6), N(1)-Fe(1)-N(5), N(3)-Fe(1)-N(5), N(6)-Fe(1)-N(4), N(2)-Fe(1)-N(4), and N(3)-Fe(1)-N(4) differ by 10.7°, 12.08°, 13.57°, 10.41°, 15.26°, 34.68°, and 15.4°, respectively, (compared to 1.46°, 2.19°, 5.10°, 4.00°, 2.95°, 12.99°, and 7.06° for the same angles in **1**), from what is expected for a regular octahedron. The average trigonal distortion angle, Φ,[12] is 3.9° and 11.1° for **1** and **2**, respectively. These results are consistent with the different spin states observed for the two compounds because the low-spin complexes are generally more regular than their high-spin counterparts. As in **1**, the $[N(CN)_2]^-$ group is angular and nonlinear (C(61)-N(7)-C(61)′ = 130.9(7)° and N(6)-C(61)-N(7) = 168.3(5)°). Relevant crystal data and selected bond lengths and angles for **2** are presented in Table 1, and Table 2, respectively.

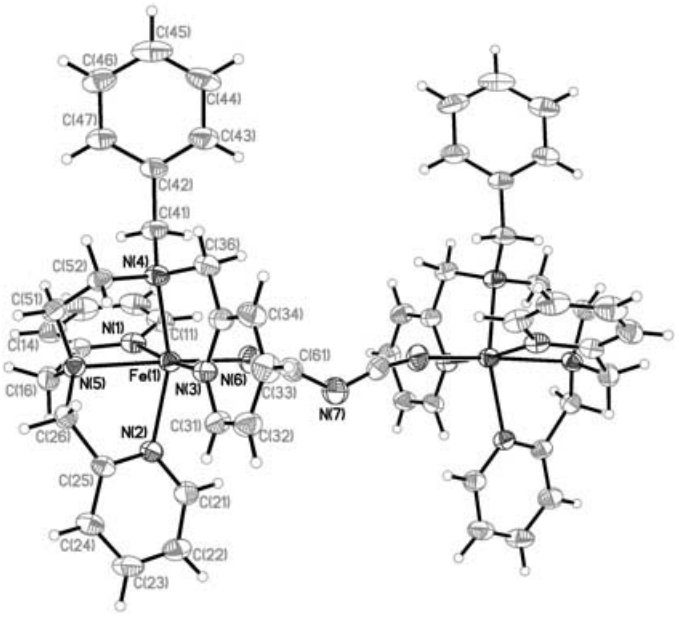

Figure 3. Molecular structure of compound **2** (displacement ellipsoids are shown at 25% probability level for clarity).

Crystal and molecular structure of 3: The crystal structure of **3** has been studied at seven selected temperatures with intervals of approximately 50 K (400 K, 350 K, 290 K, 250 K, 200 K, 150 K, and 90 K). The crystal structure of **3** remains in the triclinic space group $P\bar{1}$ throughout the temperature range studied. There are two half molecules in the asymmetric unit, both of which occupy a position such that an inversion center in the middle of the dicyanamide bridge generates the other half of the molecule. Figure 4 displays the molecular structure of one of the dinuclear units together with the atom numbering scheme, which is consistent for both dinuclear species. Viewed down the *c* axis, the molecules sit at approximately 90° to each other and can be seen to cross at the dicyanamide bridges, which are disordered (Figure 5). Directly between the center of the disordered bridges lies one of the three crystallographically inequivalent PF_6^- ions, namely that which is defined by P(3). The other two PF_6^- groups, defined by P(1) and P(2), lie in the cavities formed by the criss-crossing of the two bulky molecules.

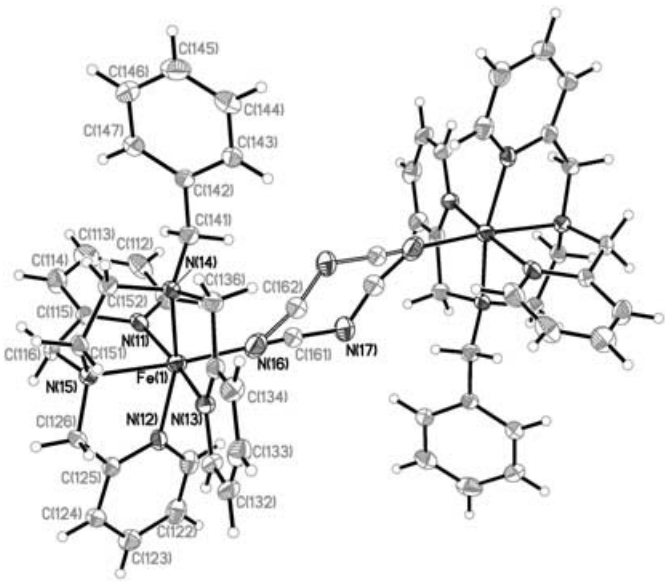

Figure 4. Molecular structure of compound **3** at 290 K (displacement ellipsoids are shown at 25% probability level for clarity). The second crystallographically inequivalent half molecule is numbered so that the first numerical digit of the atom label changes from 1 to 2 (thus N(11) becomes N(21) and C(111) becomes C(211)).

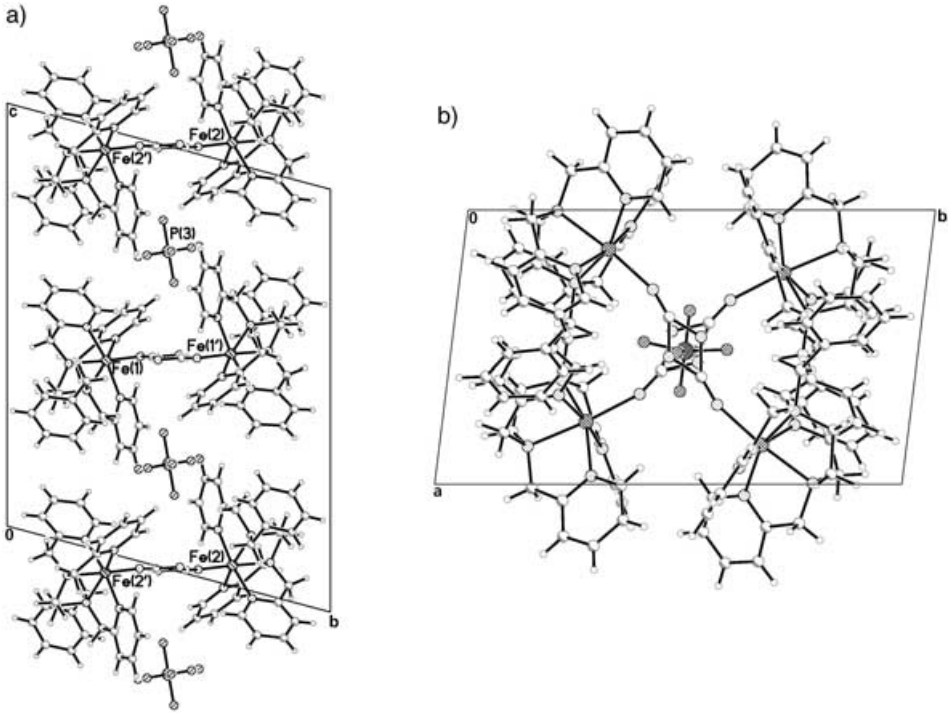

Figure 5. a) Side and b) top perspectives of the molecular packing of **3** at 400 K.

The molecular structure of **3** may be described in the same way as **2**. The iron atoms are in a distorted octahedral environment and the Fe–N bond lengths to the bztpen ligand are much longer than those to the dicyanamide bridges (Fe(1)–N(16), Fe(2)–N(26), see Table 3). The mean Fe–N bond lengths and the octahedral volumes (calculated with IVTON[13] and included in Table 3), clearly indicate that both iron centers are essentially in the high-spin state at 400 K. A comparison of the coordination core [FeN_6] for **1**–**3** demonstrates that the average Fe–N bond lengths for **3** are smaller than those seen in **2**. The average trigonal distortion angle, Φ[12] is 5.5° and 5.8° at 400 K for Fe(1) and Fe(2), respectively; values that are also between those observed for **1** and **2**, indicating an intermediate distortion of the octahedra in **3**. The same conclusion can be drawn, for instance, from the angles N(12)-Fe(1)-N(11), N(15)-Fe(1)-N(16), N(11)-Fe(1)-N(15), N(13)-Fe(1)-N(15), N(16)-Fe(1)-N(14), N(12)-Fe(1)-N(14), N(13)-Fe(1)-N(14), which differ by 1.19°, 5.59°, 9.7°, 0.88°, 6.01°, 23.59°, and 11° respectively, from what would be expected for a regular octahedron. These differences are smaller than those observed in **2**.

On cooling to 350 K and 290 K, there is clearly a contraction of the FeN_6 octahedra that is typical of the type usually seen in SCO compounds. In addition, the color of the crystal has changed from pale yellow to red. The average Fe–N bond lengths and octahedral volumes at 250 K, are slightly smaller than half way between those expected for high- and low-spin iron(II) centers ($\Delta[Fe-N_{av}] = 0.070$ Å and $\Delta V[FeN_6]_{av} = 1.09$ Å^3). On cooling to 90 K, the contraction of the coordination polyhedra continues ($\Delta[Fe-N_{av}] = 0.071$ Å, and $\Delta V[FeN_6]_{av} = 1.09$ Å^3) and the crystal becomes still darker in color. The total [$Fe-N_{av}$] change between 400 K and 90 K is equal to 0.142 Å and 0.139 Å for Fe(1) and Fe(2), respectively, and is ≈0.06 Å smaller than that usually observed for a complete iron(II) SCO;[14] a fact that may be related to the more rigid nature of the pentadentate bztpen ligand. However, the partial [$Fe-N_{av}$] variations observed for each transition, step 1 (400–250 K) and step 2 (250–90 K), are very similar, which suggests a similar extent of spin conversion in each step. Particularly sensitive to the spin state and to the occurrence of two steps is the angle N(12)-Fe(1)-N(14) and the homologous N(22)-Fe(2)-N(24) (Table 4), which increase by 10.51° for site 1 and 11.52° for site 2, in accordance with the increased regularity on changing from the HS state (400 K) to the LS state (90 K). The average trigonal distortion angle is very similar for Fe(1) and Fe(2). It has a value between those observed for **1** and **2**. This angle is also sensitive to the spin conversion and decreases as the LS state is

Table 3. Fe–N bond lengths [Å] and octahedral volumes [Å^3] for **3**.

	400 K	350 K	290 K	250 K	200 K	150 K	90 K
Fe(1)–N(11)	2.143(6)	2.127(5)	2.073(4)	2.058(5)	2.052(5)	2.008(5)	1.985(4)
Fe(1)–N(12)	2.104(6)	2.112(5)	2.062(5)	2.047(5)	2.033(5)	1.992(5)	1.966(4)
Fe(1)–N(13)	2.173(6)	2.153(5)	2.092(4)	2.085(5)	2.074(5)	2.028(4)	1.966(4)
Fe(1)–N(14)	2.263(10)	2.203(5)	2.156(4)	2.143(5)	2.140(5)	2.105(5)	2.082(4)
Fe(1)–N(15)	2.152(10)	2.169(5)	2.124(4)	2.116(4)	2.102(4)	2.049(4)	2.014(4)
Fe(1)–N(16)	2.071(14)	2.067(6)	2.032(6)	2.017(7)	2.007(7)	1.992(6)	1.986(4)
average	2.146(28)	2.134(13)	2.086(12)	2.073(10)	2.064(12)	2.027(13)	2.004(15)
O_h volume	12.84(6)	12.67(5)	11.89(5)	11.69(4)	11.63(4)	10.97(4)	10.61(4)
Fe(2)–N(11)	2.141(7)	2.120(5)	2.060(5)	2.049(5)	2.048(5)	1.996(4)	1.978(4)
Fe(2)–N(12)	2.101(7)	2.088(5)	2.053(4)	2.043(5)	2.034(5)	1.998(4)	1.958(4)
Fe(2)–N(13)	2.167(7)	2.154(5)	2.097(4)	2.086(5)	2.072(5)	2.019(4)	1.999(4)
Fe(2)–N(14)	2.222(10)	2.212(5)	2.162(4)	2.153(5)	2.149(4)	2.097(4)	2.078(4)
Fe(2)–N(15)	2.183(9)	2.184(5)	2.134(4)	2.123(4)	2.111(4)	2.039(4)	2.021(4)
Fe(2)–N(16)	2.076(12)	2.090(7)	2.046(7)	2.026(8)	2.023(7)	2.010(5)	1.997(5)
average	2.143(9)	2.137(4)	2.088(11)	2.076(12)	2.069(12)	2.024(15)	2.004(13)
O_h volume	12.76(6)	12.71(5)	11.92(5)	11.73(4)	11.55(4)	10.92(4)	10.63(4)

Table 4. Selected structural parameters for **3**.

	N(12)-Fe1-N(14) [°]	N(22)-Fe2-N(24) [°]	Trigonal distortion	
			Fe(1)	Fe(1)
400 K	156.4(3)	155.7(3)	5.50	5.85
350 K	157.54(18)	157.80(19)	5.26	5.20
290 K	160.31(15)	160.19(16)	4.65	4.75
250 K	160.99(16)	161.09(17)	4.47	4.59
200 K	161.77(16)	161.72(17)	4.31	4.44
150 K	164.22(16)	165.26(17)	4.11	3.95
90 K	166.95(14)	167.23(15)	3.78	3.73

populated (Table 4). It is important to note that all these structural modifications upon spin conversion are comparable (within error) for the two independent iron(II) centers, indicating that both independent dinuclear units undergo spin crossover simultaneously.

In addition to the changes in the iron octahedra, there are also changes in the disorder of the PF_6^- counterions (defined with reference to the central phosphorus atom) and in the behavior of the dicyanamide bridging ligand. While the thermal motion of all atoms is large at high temperatures, P(1) was considered to be ordered throughout, whereas P(2) and P(3) are both disordered. The disorder in P(2) was modeled with two orientations of equal occupancy at 400 K, decreasing fairly linearly to the occupancy ratio 0.85:0.15 at 90 K. In contrast, in P(3), the disordered components remain equally occupied in the temperature interval 400–290 K, with the occupancy of one component decreasing approximately linearly to 0.75:0.25 between 250 K and 90 K. This suggests that the change in the disorder is related to the second step of the transition.

The changes in the dicyanamide bridge seem less apparent at first. At 400 K, only the central nitrogen atom is modeled as disordered. On cooling to 290 K, this disorder appears to spread to the adjacent carbon atoms. This could, however, merely be an effect caused by the reduction of thermal motion leading to data with a higher resolution. A comparison of the thermal motion of the terminal nitrogen atoms of the dicyanamide bridge, that is, those ligating the iron centers, shows that there is a change on cooling (Figure 6). In general, thermal motion should decrease linearly with cooling.[15] Given the similar atom conditions, the thermal motion should be comparable. In **3**, the thermal motion of the ligating nitrogen atoms of the bztpen ligand decrease approximately linearly, and all within error. However, the thermal parameters for N(16) and N(26) (both part of the dicyanamide bridging ligands) do not follow this trend. It is difficult to be certain what is happening at high temperatures owing to considerable

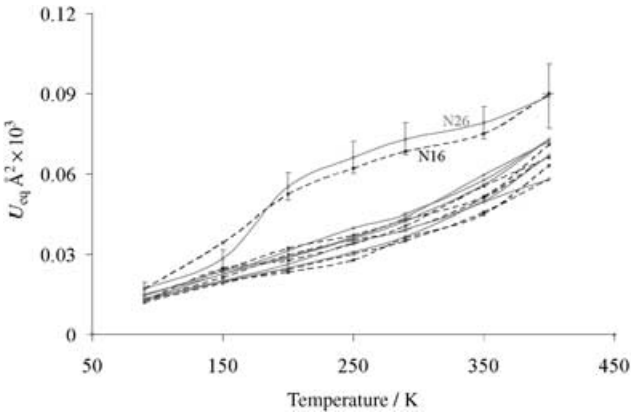

Figure 6. U_{eq} vs. temperature for the ligating nitrogen atoms in **3**. Those ligating Fe(1) are shown in black with a broken line and those ligating Fe(2) in grey with a solid line (to guide the eye). The behavior of the dicyanamide atoms N(16) and N(26) isolates them from the remaining nitrogen atoms. The largest esds are shown.

errors. While it is clear that the atomic displacement for N(16) and N(26) is comparable to that of the bztpen nitrogen atoms at low temperatures, this is not the case at high temperatures. Indeed, U_{eq} for N(16) and N(26) do not behave in the predicted linear fashion, suggesting that the disorder in the bridge also affects the terminal nitrogen atoms. This indicates that at 90 K, when the compound is entirely low spin, the terminal nitrogen atoms in the bridge are static. At 400 K, it is not certain whether the disorder in the terminal nitrogen atoms is still present because the errors are large, but it is safe to assume that any disorder present includes a large dynamic component because the energy barrier between such close positions would be small and the thermal energy present at high temperatures would be large enough to enable movement between the two. At 400 K, the thermal parameters for the central nitrogen in the dicyanamide bridge are also extremely large, suggesting that the potential energy barrier between the two positions of the bridge is small enough to allow movement between the two positions. Cooling would reduce the thermal energy in the system and the disorder would begin to become static in nature. Therefore, it is probable that this change between

dynamic and static disorder in the center of the bridge is associated with the first step of the spin-crossover transition and on cooling through the second step of the transition, the disorder in the ends of the dicyanamide bridge is reduced leading to static disorder corresponding to the low-spin state.

The connection between the bridge and the transition is further confirmed by a comparison of the Fe···Fe distances across the dicyanamide bridge. In a hypothetical isolated molecule in which the dicyanamide bridge is linear and retains its orientation and geometry during the transition, there should be a difference of approximately 0.4 Å between the Fe···Fe distances seen at 400 K and 90 K (arising from a contraction of ≈0.2 Å for the irons at each end of the dicyanamide ligand). In the case of **3**, the change in the Fe–N bond lengths arising from the spin transition are considerably less than 0.2 Å (0.085 Å for Fe(1)–N(16) and 0.079 Å for Fe(2)–N(26)), but they should still lead to an average contraction of the Fe···Fe distances of 0.164 Å. However, the Fe···Fe distance changes very little during the transition (−0.037 Å for Fe(1) and +0.020 Å for Fe(2)), which is caused by a gradual increase in the N(16)···N(16) and N(26)···N(26) distances of approximately 0.15 Å between 400 K and 90 K owing to a decrease in the N···N···N angle (from an average of 150(1) to 143(2)°).

Finally, it is interesting to point out the different relative orientation of each of the $\{Fe(bztpen)\}^{2+}$ halves with respect to the dicyanamide bridge for **2** and **3**. As shown in Figure 3, the pendent phenyl rings in **2** are on the same side of the molecule to give a *cis*-like conformation, while in **3** they point in opposite directions to give a *trans*-like conformation.

Studies in solution: The cyclic voltammograms recorded for complexes **1**–**3** in acetonitrile are displayed in Figure 7. The potentials of **2** and **3** versus Fc/Fc^+ were virtually the same with two quasireversible oxidations $E^1_{1/2} = 0.353$ and 0.350 V and $E^2_{1/2} = 0.577$ and 0.576 V (for **2** and **3**, respectively), while only one reversible oxidation was observed for **1** at $E_{1/2} = 0.344$ V. These results in conjunction with the UV/Vis behavior (see below) confirm that the coordination sphere of each Fe in all the complexes remains intact in solution. They also confirm that the dinuclear nature of **2** and **3** is retained in solution because the two redox potentials corresponding to the Fe^{III}/Fe^{II} and Fe^{III}/Fe^{III} species are observed. The difference between the two potentials $\Delta E_p = E^1_{1/2} - E^2_{1/2} = 0.224$ V and 0.226 V. This corresponds to a value of the equilibrium constant $K_c = 6.26\times10^3$ and 6.77×10^3 for **2** and **3** respectively, where K_c is defined according to Equation (6):

$$K_c = \frac{[Fe^{III}-Fe^{II}]^2}{[Fe^{III}-Fe^{III}][Fe^{II}-Fe^{II}]} \quad (6)$$

for the equilibrium [Eq. (7)]:

$$Fe^{III}-Fe^{III} + Fe^{II}-Fe^{II} \overset{K_c}{\rightleftharpoons} 2\,Fe^{II}-Fe^{III} \quad (7)$$

Analysis of the behavior of the voltamperometric function of **2** and **3** shows an important depletion of the intensity in the second process, which is probably caused by the influence of the first redox process on the second.

The magnetic properties of **2** and **3** were measured in $[D_6]$acetone by the Evans method in the temperature range 180–330 K.[16] The results are shown in Figure 8a and b. As the temperature decreases, the $\chi_M T$ product changes from 5.23 $cm^3 K mol^{-1}$ and 5.84 $cm^3 K mol^{-1}$ to 0.92 $cm^3 K mol^{-1}$ and 1.52 $cm^3 K mol^{-1}$ for **2** and **3**, respectively. This continuous decrease in $\chi_M T$ is consistent with a spin conversion taking place in solution. Experimental and calculated data have been fitted as described previously. The lack of two steps in solution makes it possible to consider the occurrence of only the global transformation HS–HS⇄LS–LS, characterized by the constant K_2. The $\chi_M T$ product can be obtained from Equation (8), where $(\chi_M T)_{HH}$ has been considered as an adjustable parameter.

$$\chi_M T = \frac{K_2(\chi_M T)_{HH}}{1 + K_2} \quad (8)$$

To obtain a good fit, the parameter f_{HS} has been included, which accounts for the HS molar fraction of species that

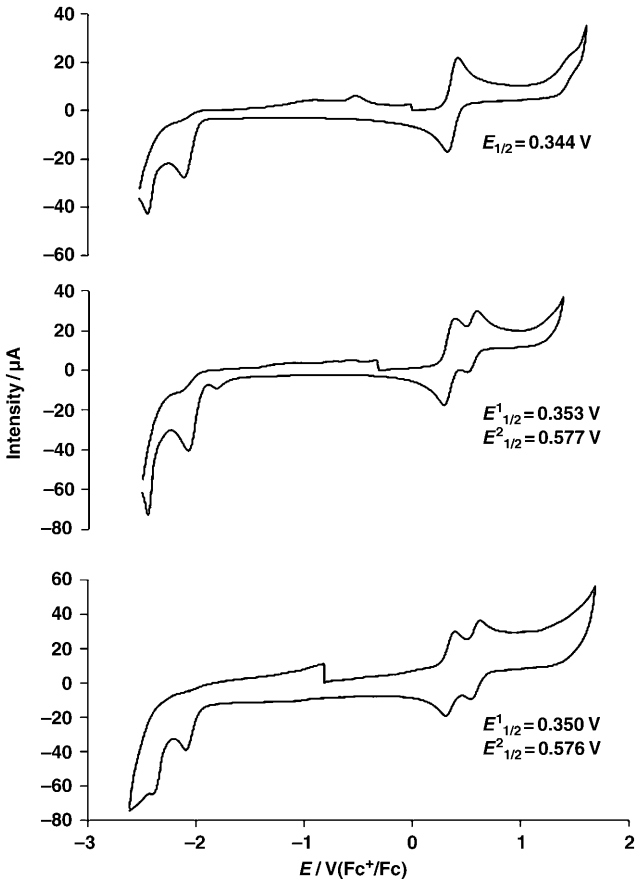

Figure 7. Cyclic voltammograms, recorded in CH_3CN, of **1** (top), **2** (middle), **3** (bottom).

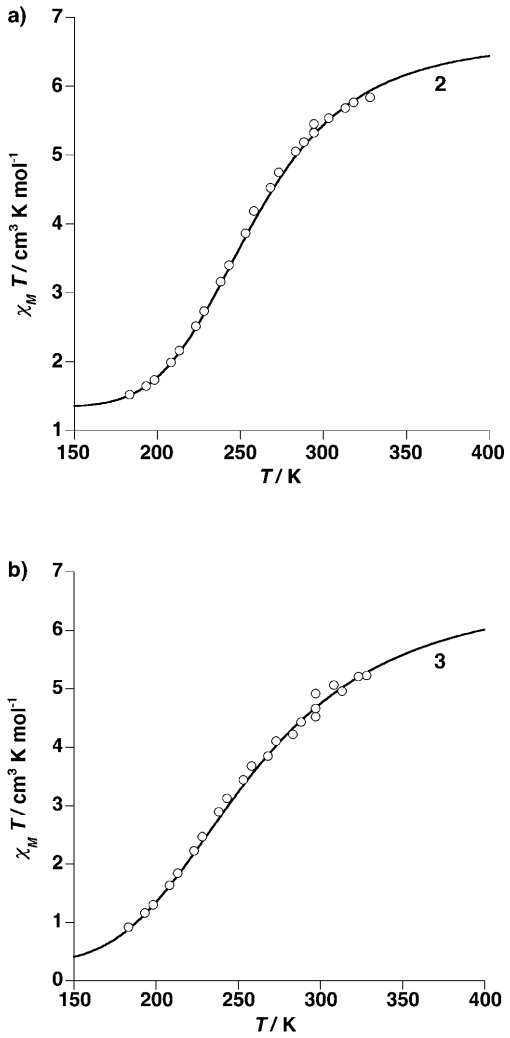

Figure 8. Magnetic properties in liquid solution state. $\chi_M T$ versus T plots for compounds **2** (top) and **3** (bottom). The solid lines represent the best fit between calculated and experimental data.

does not undergo spin conversion. Satisfactory simulations are obtained for $T_c = 258$ K, $\Delta S = 70\,J\,K^{-1}\,mol^{-1}$ ($\Delta H \approx 18.1\,kJ\,mol^{-1}$), $(\chi_M T)_{HH} = 6.7\,cm^3\,K\,mol^{-1}$ and $f_{HS} = 0.20$ for **2**, and $T_c = 252$ K, $\Delta S = 50\,J\,K^{-1}\,mol^{-1}$ ($\Delta H = 12.6\,kJ\,mol^{-1}$), $(\chi_M T)_{HH} = 6.5\,cm^3\,K\,mol^{-1}$ and $f_{HS} = 0.046$ for **3**.

The electronic spectra of **1**–**3**, dissolved in acetonitrile (see the Supporting Information), show that **2** and **3** exhibit virtually identical UV/Vis spectra with a strong absorption at $\lambda = 391$ nm with $\varepsilon = 11537\,L\,cm^{-1}\,mol^{-1}$ and $12294\,L\,cm^{-1}\,mol^{-1}$ for **2** and **3** respectively, and a weaker absorption at $\lambda = 536$ nm with $\varepsilon = 185\,L\,cm^{-1}\,mol^{-1}$ for both. On the other hand, **1** shows both absorption bands centered at $\lambda = 393$ and 529 nm with $\varepsilon = 2491$ and $60.2\,L\,cm^{-1}\,mol^{-1}$, respectively. The d–d absorption bands of these three complexes are centered at 863 nm ($11587.5\,cm^{-1}$) for **2** and **3** with $\varepsilon = 25\,L\,cm^{-1}\,mol^{-1}$ and $22\,L\,cm^{-1}\,mol^{-1}$ for **2** and **3** respectively, while in **1**, the d-d absorption band is at 860 nm ($11628\,cm^{-1}$ with $\varepsilon = 15.6\,L\,cm^{-1}\,mol^{-1}$).

Discussion

Synthetic approach: The synthesis and characterization of the system $[Fe(tpen)](ClO_4)_2 \cdot n\,H_2O$, where tpen is the hexadentate ligand *N*,*N*,*N*′,*N*′-tetrakis(2-pyridylmethyl)-1,2-ethylenediamine, was first reported more than ten years ago.[17] The anhydrous and hydrate ($n = {}^2/_3$) derivatives are essentially LS at 300 K, but show the onset of a spin equilibrium at higher temperatures that is much more marked for the hydrated compound ($T_c \approx 365$ K). This derivative shows the singularity of undergoing a fast spin-crossover transition with respect to the ^{57}Fe Mössbauer timescale (10^7–$10^8\,s^{-1}$). From a synthetic viewpoint, it is clear that the use of hexadentate ligands, such as tpen, are not conducive to the investigation of new polynuclear SCO complexes because, on one hand, they form strong ligand field LS iron(II) complexes, and on the other hand, labilization of at least one coordination site in the precursor complex to insert a potential bridging ligand is difficult. Interestingly, the search for new synthetic analogues of the active intermediate in the reaction cycle of bleomycin[18] has led to the synthesis of new ligands derived from tpen. These include *N*-methyl-, *N*-ethyl-, or *N*-benzyl-*N*,*N*′,*N*′-tetrakis(2-pyridylmethyl)-1,2-ethylenediamine, generically referred to as Rtpen.[19] The use of such pentadentate aminopyridyl ligands based on ethylenediamine has allowed the formation of hexacoordinated iron(II) complexes whose spin state depends on the nature of the monodentate ligand in the sixth coordination site (i.e. solvent, halide, or pseudohalide groups). Therefore, in this context, we decided to investigate the interaction between the complex $[Fe(bztpen)S]^{2+}$ (S = H_2O or MeOH) and the bridging dicyanamide anion.

The mononuclear compound **1** precipitates as red prismatic diamagnetic single crystals from appropriate stoichiometric amounts of reactants. The crystal structure and the solid state magnetic behavior of **1** indicate the presence of LS iron(II). This suggests that, in this case, the formal replacement of one pyridyl group by one dicyanamide ligand does not trigger the weakening of the ligand field at the iron(II) site that is necessary in order to observe SCO phenomena. In this respect, it is worth mentioning that only one example of an iron(II) SCO compound containing the dicyanamide anion as a ligand has been reported to date, namely $[Fe(abpt)_2(dca)_2]$ (abpt = 4-amino-3,5-bis(pyridin-2-yl)-1,2,4-triazole).[20] From a comparison of this derivative with the related $[Fe(abpt)_2(NCX)_2]$ (X = S or Se), it is clear that the ligand field strength of dicyanamide is markedly weaker than that of the pseudohalides NCS^- and $NCSe^-$.[21]

The formation of **2** or **3** takes place from a dca^-:$[Fe(bztpen)S]^{2+}$ ratio close to 1:2, in the presence of an excess of PF_6^-. Complex **2** precipitates as a pale yellow, microcrystalline powder, while **3** needs at least 36 h to grow as brown prismatic single crystals. The most remarkable structural difference between both dimers is the orientation of the phenyl rings with respect to one another. While the phenyl groups appear to be in a *cis* conformation in **2**, the *trans* conformation is retained in **3**. Most probably, the formation

of **2** is controlled kinetically, whereby **3** is the thermodynamically stable species. The coordination core of **2** (at 300 K) is considerably more distorted than that of **3** (at 400 K, where it is essentially HS). These structural differences are reflected in the differences in magnetic behavior observed for **2** and **3** in the solid state. Compound **2** displays HS–HS behavior in the whole range of temperatures. Similarly, recent work aimed at synthesizing dca-bridged dinuclear Fe^{II} SCO compounds led to double dca bridges and HS–HS behavior.[22]

Two-step SCO behavior: Two-step SCO transitions are scarce and only a few well-documented examples have been reported. The mononuclear complex $[Fe(2\text{-pic})_3]Cl_2 \cdot EtOH$ (2-pic = 2-picolylamine) was the first example of a two-step SCO and is generally considered prototypical.[23] This compound contains only one crystallographically unique iron center in both the HS state and the LS state;[24] however, the nature of the plateau has been subject of study for more than 20 years.[25] From a theoretical viewpoint it was believed that the plateau reflected the existence of short-range interactions responsible for the occurrence of clusters defined by LS–HS pairs. However, Bürgi and co-workers used synchrotron radiation to reveal the existence of an intermediate phase that defines the plateau.[26] Furthermore, in contrast to previous studies, it clearly establishes that long-range order occurs in the plateau defined by infinite -[LS–HS-LS]- chains of $[Fe(2\text{-pic})_3]^{2+}$ molecules.[8] Within each chain, the complex molecules strongly interact with each other through hydrogen bonds between the Cl^- ions and the EtOH molecules. This is in contrast to the situation in the two-step spin transition exhibited by the monomeric compound {Fe[5-NO_2-sal-N(1,4,7,10)]}, where 5-NO_2-sal-N-(1,4,7,10) is a hexadentate ligand synthesized from the condensation of 5-NO_2-salicylaldehyde with 1,4,7,10-tetraazadecane). In this complex, the transition is associated with the existence of two different iron sites, which allows the identification of two equally distributed sets of molecules in the crystal.[27]

A similar phenomenology may be observed for dinuclear compounds. As mentioned in the introduction, step-wise transitions have been observed for the $\{[Fe(L)(NCX)_2]_2(\mu\text{-bpym})\}$ family[3] and the compound $\{[Fe(phdia)(NCS)_2]_2(\mu\text{-phdia})\}$.[4] The $\{[Fe(bpym)(NCX)_2]_2(\mu\text{-bpym})\}$ (X = S or Se) derivative is HS and displays intramolecular antiferromagnetic coupling. However, this coupling can be suppressed by the appropriate choice of the peripheral ligands owing to the occurrence of thermal SCO in one or even both iron centers. Magnetic studies performed on these compounds under pressure have nicely demonstrated that the ligand field strength can be tuned in a much more efficient manner. Thus, $\{[Fe(bpym)(NCX)_2]_2(\mu\text{-bpym})\}$ has been observed to a undergo thermal spin transition in only one of the two centers under hydrostatic pressure.[3d] This is unusual given that, according to an X-ray structure determination, both centers have entirely equivalent surroundings,[3b] as is the case in **3**. The appearance of the spin transition in only one center of the bridged pair, concluding in a plateau with all pairs present in LS–HS pair formation, supports the suggestion that LS–HS pair formation is a preferred process arising from a synergetic effect between intramolecular and cooperative intermolecular interactions.[3c] Similar behavior has been observed for $\{[Fe(bpym)(NCSe)_2]_2bpym\}$ at atmospheric pressure.[3d] A method has recently been developed for direct monitoring of the spin state and the magnetic coupling in dinuclear iron(II) compounds.[3f] This method involves Mössbauer measurements carried out in an external magnetic field (5 T). The species HS–HS, LS–HS, and LS–LS have been identified in $\{[Fe(bpym)(NCS)_2]_2bpym\}$, $\{Fe(bpym)(NCSe)_2]_2bpym\}$, $\{[Fe(bt)(NCS)_2]_2bpym\}$, and $\{[Fe(phdia)(NCS)_2]_2(\mu\text{-phdia})\}$ at 4.2 K. Moreover, the application of applied-field Mössbauer spectroscopy to study the LIESST effect on dinuclear compounds demonstrates the effectiveness of this approach. The crystal structure of $\{[Fe(bt)(NCS)_2]_2bpym\}$ in the plateau indicates that standard X-ray diffraction experiments cannot distinguish between the two iron(II) sites belonging to the LS–HS species,[3i] as occurred in the standard X-ray studies of $[Fe(2\text{-pic})_3]Cl_2 \cdot EtOH$. In contrast to mononuclear compounds, the plateau in dinuclear compounds may also arise from the occurrence of a 50:50 distribution of HS–HS and LS–LS dinuclear species instead of 100% of LS–HS species. This was the case recently observed by Kaizaki and co-workers for the compound $\{[Fe(4\text{-phpy})(NCBH_3)_2]_2(\mu\text{-bpypz})\}$ (4-phpy is 4-phenyl-pyridine, bipypz is 3,5-bis(2-pyridyl)pyrazolate), where the plateau is defined by an ordered distribution of HS–HS and LS–LS molecules.[6] In contrast to this, the results by Brooker, Murray, and co-workers report the first structural characterization of the LS–HS spin pair in a new dinuclear iron(II) compound, which displays a 50% conversion.[7]

As far as compound **3** is concerned, we have observed the occurrence of two crystallographically distinct dinuclear molecules in the solid state. As a consequence, the step-wise nature of the SCO could be assumed to be associated with this fact. However, our multitemperature X-ray study demonstrates that the two molecules undergo SCO simultaneously (Figure 9). We believe that a more sophisticated structural analysis, similar to that performed on $[Fe(2\text{-pic})_3]Cl_2 \cdot EtOH$, might provide evidence of the occurrence of an intermediate phase in which the LS–HS molecules exist.

Cooperative nature of the SCO: As already discussed, the two-step SCO is not an exclusive feature of dinuclear complexes. Current research in this field has afforded four new dinuclear complexes: $\{[Fe(dpa)(NCS)_2]_2(\mu\text{-bpym})\}$,[28] $\{[Fe(pypzH)(NCSe)]_2(\mu\text{-pypz})\}$ (where dpa stands for 2,2′-dipyridylamine, and pypzH and $pypz^-$ are 2-pyrazolylpyridine and its deprotonated form, respectively),[3a] and $\{[Fe(NCX)(py)]_2(\mu\text{-bpypz})_2\}$ (where X = S or BH_3).[5b,c] The μ-pypz and μ-bpypz dimers undergo relatively cooperative one-step SCO, which indicates that two-step SCO is not a property intrinsic to dinuclear species. Interestingly, the dpa-(μ-bpym) dimer seems to be the first member of the bpym-bridged dimers that apparently display only one-step behav-

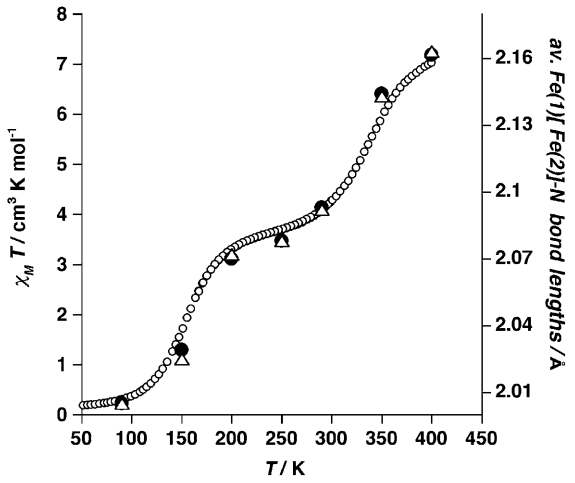

Figure 9. Correlation between the thermal dependence of the magnetic behavior and the average Fe(1)–N and Fe(2)–N bond lengths in **3**.

ior. Indeed, the dpa-μ-bpym derivative undergoes a very poorly cooperative SCO transition characterized by an unusually shaped $\chi_M T$ vs T curve. In our opinion, this fact could indicate the occurrence of two unresolved spin transitions that spread over a range of more than 300 K. In the light of this phenomenon, it is difficult to assess the factors that control the SCO regime in dinuclear complexes because it seems to depend on a delicate balance between intra- and intermolecular elastic, and perhaps electronic, interactions.

The cooperativity that leads to the propagation of the spin-crossover transition through a crystal is dependent on the transmission of elastic interactions through the crystal lattice mediated by intermolecular interactions. In this respect, the geometrical intramolecular changes associated with the SCO demonstrate that **3** has a very flexible structure. For instance, the $[FeN_6]$ core experiences noticeable angular changes in addition to the Fe–N bond length changes. Furthermore, by bending, the flexible dicyanamide bridge absorbs some of the effects of the spin change because no significant shortening of the Fe···Fe intra-dimer distance is observed upon SCO. In addition, the crystal packing clearly shows that the dinuclear species are relatively well isolated because no strong intermolecular contacts between complex molecules (coupled directly or through PF_6^- groups) are observed. These facts explain why the transition is poorly cooperative; however, it is difficult to ascertain why this system displays a step-wise transition and whether electronic communication may play a role in it. These results suggest that the lack of cooperativity does not play any substantial role in the observation of two-step SCO in **3**.

Disorder and SCO: The interplay between order–disorder and SCO phenomena has been discussed for many years. For instance, disorder was suggested to be related to the nature of the SCO in $[Fe(2\text{-pic})_3]Cl_2 \cdot EtOH$.[24b] As noted above, the complex cations $[Fe(2\text{-pic})_3]^{2+}$ strongly interact with each other through hydrogen bonds between Cl^- anions and EtOH solvent molecules. Thermal ordering of the ethanol molecules was considered to be a trigger of the spin change. Similarly, order–disorder transitions in solvent molecules have been associated with the SCO in $[Fe(dppen)_2Cl_2] \cdot 2S$ (where dppen is *cis*-1,2-bis(diphenylphosphino)ethylene, from Mössbauer studies[29a] for S = $(CH_3)_2CO$, and from X-ray studies[29b] for S = $CHCl_3$). Order–disorder transitions in uncoordinated anions have also received much attention.[30] The complex $[Fe(dapp)(abpt)](ClO_4)_2$ (dapp = bis(3-aminopropyl)(2-pyridylmethyl)amine) is a recent example which not only exhibits a concomitance between the order–disorder transition of the perchlorate ions and the SCO, but also represents the first observation of such a transition involving the ligand directly coordinated to the iron(II) atom.[30e] Similarly, in the case of **3** we have also observed the occurrence of different kinds of disorder, which change during the spin conversion and involve both the PF_6^- counterions and the dicyanamide bridging ligand. While the thermal disorder of the P(2) PF_6^- changes linearly from an occupation ratio 0.5:0.5 at 400 K to 0.85:0.15 at 90 K, the P(3) PF_6^- changes from the occupation ratio 0.5:0.5 at 250 K to 0.75:0.25 at 90 K, and coincides with the second spin change. These observations may suggest that the two-step character of the SCO could be triggered by order–disorder transitions in **3**. While order–disorder transitions exhibited by counterions are not uncommon, similar structural changes in ligands are considerably more unusual.[30e] In the case of **3**, the changes in the counterions appear to be coupled with changes to the bridging dicyanamide. Given the quality of the data at high temperature, it is difficult to be certain of exactly what is happening. However, it seems clear that there is dynamic disorder at 400 K which could involve rotation of the $[N(CN)_2]^-$ ligand. This is reduced at the plateau and becomes static on cooling to 90 K. The location of the P(3) PF_6^- between the crossing dicyanamide ligands (Figure 5) suggests that there may be a connection between the counterion disorder and the disorder in the bridge; however, this is difficult to confirm.

Solution studies: Most dinuclear systems synthesized so far are insoluble or unstable in solution, but this is not the case for **2** and **3** and electrochemical studies have demonstrated the stability of these dinuclear complexes in solution. These studies along with the UV/Vis study, confirm that the coordination sphere of each iron atom in all the complexes remains intact in solution. The observed influence of the first redox process on the second, can be attributed to the withdrawal of electronic density from the iron that is oxidized first by the second. This phenomenon is commonly observed in systems referred to as molecular wires. All this and the magnitude of the splitting observed in the couples indicates a large degree of electronic coupling between the iron atoms through the dicyanamide bridge in the spin-crossover units, which is comparable with that observed in biferrocenes with steric hindrance between substituents, that is, 2,2′-dimethyl-biferrocene (ΔE_p = 0.26 V in CH_3CN) and in α,ω-diferrocenyl cumulenes.[31]

On cooling, both compounds undergo a very similar spin change that appears to be characterized by a single step taking place at similar characteristic temperatures (T_c). This confirms that the crystal structure is responsible for the differences between the SCO transitions in **2** and **3** in the solid state. Another interesting result is that the two transitions observed in the solid state for **3** present similar shapes compared to those observed for **2** and **3** in solution. This confirms our previous hypothesis concerning the very weak intermolecular interactions operative in **3**. A similar behavior has been observed in $[Fe(tpen)](ClO_4)_2 \cdot {}^2/_3 H_2O$ for which a rapid SCO conversion in the solid state was observed.[17]

Conclusion

Herein we have reported a novel synthetic strategy to obtain dinuclear spin crossover complexes. Starting from the monomeric precursor $\{[(Fe(bztpen)]N(CN)_2\}^+$, two isomeric forms of the first dicyanamide-bridged iron(II) dinuclear spin-crossover system $\{[(Fe(bztpen)]_2N(CN)_2\}^{3+}$ have been synthesized and characterized for the first time. One form (**3**) displays a gradual two-step spin conversion. For the second form (**2**), this conversion depends on the texture (crystalline or precipitate) and the history of the sample. Although there are two crystallographically different iron(II) atoms in **3**, the two-step conversion is not associated with this fact. Probably, the occurrence of an intermediate phase defined by 100% LS–HS molecules or by 50% HS–HS and 50% LS–LS pairs should be the origin of this observation. The stabilization of the LS–HS state seems to depend on a delicate balance between intra- and intermolecular interactions in the solid state. The electronic coupling between the iron(II) atoms through the dicyanamide bridge, observed from electrochemical measurements in solution, should favor the stabilization of the intermediate spin state.[3b] However, this state seems to succumb in acetonitrile solution, in which both forms display a similar continuous spin transition.

Experimental Section

Manipulations were performed under an atmosphere of argon by means of standard Schlenk techniques. Commercially available chemicals were used without prior purification. The bztpen ligand was synthesized according to a literature procedure.[32]

Preparation of $\{Fe(bztpen)[N(CN)_2]\}PF_6 \cdot CH_3OH$ (1): A solution of bztpen (0.24 mmol) in methanol (10 mL) was added dropwise to a solution of $Fe(BF_4)_2 \cdot 6H_2O$ (0.24 mmol) in the same solvent (5 mL). To the resulting yellow solution was slowly added a freshly prepared solution of $NaN(CN)_2$ (0.71 mmol) in methanol (10 mL). The mixture was stirred for 20 min, then a solution of NH_4PF_6 (0.71 mmol) in methanol (20 mL) was added very slowly. The resulting transparent brown solution was evaporated slowly under Ar. Brown needles of **1** were collected after $\approx$36 h. Yield: 0.087 g (51%); FAB MS: *m/z*: 498 $[M-PF_6-CH_3OH-N(CN)_2+H_2O]^+$, 545 $[M-PF_6^- -CH_3OH]^+$; elemental analysis calcd (%) for $C_{30}H_{33}N_8F_6OPFe$: C 49.9, H 4.57, N 15.5; found: C 49.3, H 4.15, N 14.7; IR (KBr): $\tilde{\nu}$ = 2160, 2220, 2259 (C≡N) cm^{-1}.

Preparation of $\{[(Fe(bztpen)]_2[N(CN)_2]\}(PF_6)_3 \cdot H_2O$ (2) and $[(Fe(bztpen)]_2[N(CN)_2]](PF_6)_3$ (3): A solution of bztpen (0.24 mmol) in methanol (10 mL) was added dropwise to a solution of $Fe(BF_4)_2 \cdot 6H_2O$ (0.24 mmol) in the same solvent (5 mL). To this yellow solution was added very slowly a freshly prepared solution of $NaN(CN)_2$ (0.12 mmol) in methanol (10 mL). The mixture was stirred for 20 min, after which a solution of NH_4PF_6 (0.71 mmol) in methanol (20 mL) was added very slowly while stirring. A yellow microcrystalline powder of **2** precipitated immediately from this dark yellow mixture. Yellow crystals of **2** had formed 24 h later. Yield of powder and crystals: 0.09 g (52%); FAB MS: *m/z*: 479 $[Fe(Bztpen)+e^-]^+$, 545 $[M-Fe(bztpen)-3PF_6^- -H_2O]^+$, 1188 $[M-2PF_6^- +e^-]^+$, 1314 $[M-PF_6^- -H_2O]^+$; elemental analysis calcd (%) for $Fe_2C_{56}H_{60}F_{18}N_{13}OP_3$: C 45.5, H 4.06, N 12.3; found: C 45.8, H 4.13, N 12.3; IR (KBr): $\tilde{\nu}$ = 2203, *2253*, *2364* (C≡N) cm^{-1}. The filtered brown solution was left under Ar for 36 h. The dark brown prismatic crystals of **3** that had formed were collected over the following week. Yield: 0.04 g (23%); FAB MS: *m/z*: 479 $[M-Fe(Bztpen)-N(CN)_2-3PF_6^- +e^-]^+$, 545 $[M-Fe(bztpen)-3PF_6^-]^+$, 1188 $[M-2PF_6^- +H_2O^- +e^-]^+$, 1314 $[M-PF_6]^+$; elemental analysis calcd (%) for $Fe_2C_{56}H_{58}F_{18}N_{13}P_3$: C 46.1, H 3.97, N 12.5; found: C 45.7, H 3.85, N 12.1; IR (KBr): $\tilde{\nu}$ = 2172, 2318 (C≡N) cm^{-1}.

Physical measurements: Variable-temperature magnetic susceptibility measurements of samples consisting of small single crystals (20–30 mg) were recorded with a Quantum Design MPMS2 SQUID susceptometer equipped with a 5.5 T magnet, operating at 1 T and at temperatures from 1.8–300 K. Magnetic measurements under pressure were performed in a cylindrical hydrostatic pressure cell made of hardened beryllium bronze (1 mm in diameter and 5–7 mm in length) that was specially designed for this SQUID set up.[33] Silicone oil was used as the pressure-transmitting medium operating in the pressure range 1 bar to 12 kbar. The pressure was measured with respect to the pressure dependence of the superconducting transition temperature of a built-in pressure sensor made of high purity tin. The susceptometer was calibrated with $(NH_4)_2Mn(SO_4)_2 \cdot 12H_2O$. The variable-temperature magnetic susceptibility in solution was measured with the Evans method, in the range 183–323 K in $(CD_6)_2CO$ at a concentration of 0.01 M. Chemical shifts are referenced to tetramethylsilane (TMS). All spectra were recorded in a Varian Unity Inova 300 instrument at 300 MHz. Experimental susceptibilities were corrected for diamagnetism of the constituent atoms by the use of Pascal's constants. UV/Vis absorption spectra in solution were measured on a HP 8493 diode array spectrophotometer in CH_3CN. All λ_{max} and the corresponding molar absorptivity coefficients ε [$L cm^3 mol^{-1}$] were obtained with a statistic treatment of the absorption spectra at several concentrations. Electrochemical measurements were carried out in a potentiostat galvanostate autolab model Pgstat 30, with a three-electrode system in a 0.1 M $Bu_4N(PF_6)$ acetonitrile solution as the supporting electrolyte. A carbon glass disc (0.071 cm^2) was used as the working electrode, a Pt wire as the auxiliary electrode, and 0.1 M $(Bu_4N)Br/AgBr(s)/Ag$ was used as the reference electrode. The working electrode (C) was polished with alumina to ensure the absence of residues on the surface. All voltammograms were initiated from the null current potential (E_i = 0) and the scan was initiated in both positive and negative potential directions. In order to report the potentials used according to the IUPAC convention, voltammograms were obtained for approximately 10^{-3} M solutions of ferrocene (Fc) in a supporting electrolyte. For the working conditions, the electroactive domain was between −1.726 and 0.274 V Fc^+/Fc. The half-wave potentials were estimated from $E_{1/2} = (E_{pa} + E_{pc})/2$, where E_{pa} and E_{pc} are the anodic and cathodic peak potentials, respectively.

Single-crystal X-ray diffraction: Diffraction data of prismatic crystals of **1** and **2** were collected at 293 K with an Enraf-Nonius CAD4 diffractometer and graphite-monochromated $Mo_{K\alpha}$ radiation (λ = 0.71073 Å). The structures were solved by direct methods with SHELXS-97 and refined by full-matrix least-squares on F^2 with SHELXL-97.[34] The hydrogen atoms of the solvent molecules were located in the difference map; however, refinement was unstable so that the hydrogen atoms of CH_3OH were refined with a riding model.

Single-crystal X-ray diffraction experiments for **3** were carried out with graphite-monochromated $Mo_{K\alpha}$ radiation (λ = 0.71073 Å) on a Bruker

ProteumM diffractometer with an Apex area detector and a Bede Microsource. In general, three series of narrow ω scans (0.3°) were performed at different settings in such a way as to cover a sphere of reciprocal space to a maximum resolution of 0.75 Å. The temperature control was carried out with an Oxford Cryostream 700 series N_2 open-flow cooling device,[35] and data were collected at 400, 350, 290, 250, 200, 150, and 90 K.

In each case, the unit cell parameters were determined and refined with the SMART software[36] and the raw frame data were integrated with the SAINT program.[37] The structures were solved by direct methods and refined by full-matrix least-squares on F^2 with SHELXTL software.[38] Reflection intensities were corrected for absorption effects by numerical integration based on measurements and indexing of the crystal faces (SHELXTL software).[38]

Non-hydrogen atoms were refined anisotropically, except if there was disorder present. The two halves of the dinuclear cations are related by an inversion center; however, the central nitrogen of the dicyanamide bridging ligand occupies a position away from the symmetry position, and is therefore disordered over two positions. The distance between these two positions is sufficient to enable anisotropic refinement at all temperatures; however, at 290 K and below, the carbon atoms in the bridge were also modeled as disordered. These two positions are much closer together with a considerable amount of overlap, making anisotropic refinement impossible. Thus, at 290, 250, 200, and 150 K, the carbon atom displacements were modeled as isotropic. At 90 K, the disorder is still present, but the thermal motion is sufficiently reduced to allow refinement of anisotropic displacement parameters. In addition, there is disorder present in the PF_6^- counterions (hereafter referred to by the phosphorous atom label). In the case of the P(1), although the PF_6^- ion is clearly librating at higher temperatures, no disorder is modeled because the large displacement parameters appear to be caused only by thermal effects. This is not the case for P(2) and P(3) however. At 400 K, P(2) was modeled with two equally occupied components, rotationally offset, with the central phosphorous atom coincident. The disorder is clearly dynamic in nature, because the occupancy changes on cooling (modeled linearly) until the minor component is only 15% occupied at 90 K. The disorder in P(3) is also rotational in nature, but is more structured as the rotation axis is coincident with the F(35)–P(3)/P(3)–F(36) bonds, so that at 400 K, a total of eight equatorial fluorine atoms were modeled with two equally occupied components. Similar to P(2), there is clearly a dynamic aspect to the disorder, but in contrast, the disordered P(3) components were modeled as equally occupied from 400 K to 250 K, after which the occupancy was also modeled as reducing linearly. At low occupancies, anisotropic refinement of the thermal motion leads to infeasible displacement parameters for the fluorine atoms. Therefore, for P(2), the minor component was modeled as isotropic at 250 K and below, while for P(3) this is the case only at 150 K and 90 K. In many cases, restraints were necessary to maintain sensible octahedral geometries, and in general, these were used to restrain similar distances to a consistent value. Hydrogen atoms were positioned geometrically and refined with a riding model. Selected crystallographic data are presented in Table 1.

CCDC 263310–CCDC-263318 contain the supplementary crystallographic data for this paper. These data can be obtained free of charge from the Cambridge Crystallographic Data Centre via www.ccdc.cam.ac.uk/data_request/cif.

Acknowledgements

We are grateful for financial support from the Spanish DGICYT through Project CTQ 2004–03456/BQU and The Royal Society for a Study Visit and a Joint Project award. In addition, we thank the Universitat de València for a predoctoral fellowship (N.O.V.) and the EPSRC for a postgraduate studentship (A.L.T.). We are grateful to Q. Rosa Isela del Villar for NMR spectra studies and to Dr. V. Ksenofontov for preliminary Mössbauer studies of compound **3**.

[1] *Spin Crossover in Transition Metal Compounds* (Eds.: P. Gütlich, H. A. Goodwin), *Top. Curr. Chem*. 233–235, Springer, Berlin, **2004**.
[2] J. A. Real, J. Zarembowitch, O. Kahn, X. Solans, *Inorg. Chem.* **1987**, *26*, 2939–2943.
[3] a) J. A. Real, A. B. Gaspar, M. C. Muñoz, P. Gütlich, V. Ksenofontov, H. Spiering, *Top. Curr. Chem.* **2004**, *233*, 167–193; b) J. A. Real, H. Bolvin, A. Bousseksou, A. Dworkin, O. Kahn, F. Varret, J. Zarembowitch, *J. Am. Chem. Soc.* **1992**, *114*, 4650–4658; c) J. A. Real, I. Castro, A. Bousseksou, M. Verdaguer, R. Burriel, M. Castro, J. Linares, F. Varret, *Inorg. Chem.* **1997**, *36*, 455–464; d) V. Ksenofontov, A. B. Gaspar, J. A. Real, P. Gütlich, *J. Phys. Chem. B* **2001**, *105*, 12266–12271; e) V. Ksenofontov, H. Spiering, S. Rieman, Y. Garcia, A. B. Gaspar, N. Moliner, J. A. Real, P. Gütlich, *Chem. Phys. Lett.* **2001**, *348*, 381–386; f) J. F. Létard, J. A. Real, N. Moliner, A. B. Gaspar, L. Capes, O. Cador, O. Kahn, *J. Am. Chem. Soc.* **1999**, *121*, 10630–10631; g) G. Chastanet, A. B. Gaspar, J. A. Real, J. F. Létard, *Chem. Commun.* **2001**, 819–820; h) A. B. Gaspar, A. L. Thompson, M. C. Muñoz, V. Ksenofontov, A. E. Goeta, P. Gütlich, J. A. Real, unpublished results; i) A. L. Thompson, *Structure-Property Correlations in Novel Spin Crossover Compounds*, Ph. D. Thesis **2004**; j) S. Brooker, P. G. Plieger, B. Moubaraki, K. S. Murray, *Angew. Chem.* **1999**, *111*, 424–426; *Angew. Chem. Int. Ed.* **1999**, *38*, 408–410; .
[4] V. Ksenofontov, A. B. Gaspar, V. Niel, S. Reiman, J. A. Real, P. Gütlich, *Chem. Eur. J.* **2004**, *10*, 1291–1298.
[5] a) B. A. Leita, B. Moubaraki, K. S. Murray, J. P. Smith, J. D. Cashion, *Chem. Commun.* **2004**, 156–157; b) N. Suemura, M. Ohama, S. Kaizaki, *Chem. Commun.* 2001, 1538–1539; c) K. Nakano, N. Suemura, S. Kawata, A. Fuyuhiro, T. Yagi, S. Nasu, S. Morimoto, S. Kaizaki, *Dalton Trans.* **2004**, 982–988.
[6] K. Nakamo, S. Kawata, K. Yoneda, A. Fuyuhiro, T. Yagi, S. Nasu, S. Morimoto, S. Kaizaki, *Chem. Commun.* **2004**, 2892–2893.
[7] K. S. Murray, B. A. Leita, B. Moubaraki, D. Offermann, S. Brooker, M. H. Klingele, J. G. Cashion, *Chem. Commun.* **2005**, 987–989.
[8] a) D. Chernyshov, M. Hostettler, K. W. Törnroos, H-B Bürgi, *Angew. Chem.* **2003**, *115*, 3955–3960; *Angew. Chem. Int. Ed.* **2003**, *42*, 3825–3830; b) C. M. Grunert, J. Schweifer, P. Weiberger, W. Linert, K. Mereiter, G. Hilscher, M. Müller, G. Wiesinger, P. J. Koningsbruggen, *Inorg. Chem.* **2004**, *43*, 155–165.
[9] a) V. Niel, A. L. Thompson, A. E. Goeta, C. Enachescu, A. Hauser, A. Galet, M. C. Muñoz, J. A. Real, *Chem. Eur. J.* **2005**, *11*, 2047–2060; b) M. Yamada, M. Ooidemizu, Y. Ikuta, S. Osa, N. Matsumoto, S. Iijima, M. Kojima, F. Dahan, J. P. Tuchagues, *Inorg. Chem.* **2003**, *42*, 8406–8416.
[10] M. Ruben, E. Breuning, J. M. Lehn, V. Ksenofontov, F. Renz, P. Gütlich, G. B. M. Vaughan, *Chem. Eur. J.* **2003**, *9*, 4422–4429.
[11] O. Kahn, *Molecular Magnetism*, VCH, New York, **1993**.
[12] The average trigonal distortion parameter, Φ, can be defined as $\Phi = \sum_{1}^{24} (|60-\theta|)/24$, where θ represents the trigonal angles defined by two opposed faces of the octahedron, giving a total of 24 trigonal angles (see the Supporting Information). This definition is similar to that reported in ref. [14]; however, the main difference is that only two opposed faces of the octahedron where considered in ref. [14], whereas our definition takes all possible combinations into account.
[13] T. Balic-Zunic and I. Vickovic, *J. Appl. Crystallogr.* **1996**, *29*, 305–306.
[14] E. König, *Prog. Inorg. Chem.* **1987**, *35*, 527.
[15] B. T. M. Willis, A. W. Pryor, *Thermal Vibrations in Crystallography*, Cambridge Press, Great Britain **1975**.
[16] a) D. F. Evans, *J. Chem. Soc.* **1959**, 2003–2005; b) D. H. Live, S. I. Chan, *Anal. Chem.* **1970**, *42*, 791–792; c) D. Ostfeld, I. A. Cohen, *J. Chem. Educ.* **1972**, *49*, 829;; d) E. M. Shubert, *J. Chem. Educ.* **1992**, *69*, 62–69.
[17] H. R. Chang, J. K. McCusker, H. Toftlund, S. R. Wilson, A. X. Trautwein, H. Winkler, D. N. Hendrickson, *J. Am. Chem. Soc.* **1990**, *112*, 6814–6827.

[18] A. J. Simann, S. Döpner, F. Banse, S. Bourcier, G. Boucchoux, A. Boussac, P. Hildebrand, J. J. Girerd, *Eur. J. Inorg. Chem.* **2000**, 1627–1633.
[19] a) I. Bernal, I. M. Jensen, K. B. Jensen, C. J. McKenzie, H. Toftlund, J. P. Tuchagues, *J. Chem. Soc. Dalton Trans.* **1995**, 3667–3675; b) K. B. Jensen, C. J. McKenzie, L. P. Nielsen, J. Z. Pedersen, H. M. Svendsen, *Chem. Commun.* **1999**, 1313–1314.
[20] N. Moliner, A. B. Gaspar, M. C. Muñoz, V. Niel, J. Cano, J. A. Real, *Inorg. Chem.* **2001**, *40*, 3986–3991.
[21] a) N. Moliner, M. C. Muñoz, P. J. van Koningsbruggen, J. A. Real, *Inorg. Chim. Acta* **1998**, *274*, 1–6; b) N. Moliner, M. C. Muñoz, S. Létard, J. F. Létard, X. Solans, R. Burriel, M. Castro, O. Kahn, J. A. Real, *Inorg. Chim. Acta* **1999**, *291*, 279–288.
[22] S. R. Batten, J. Bjernemose, P. Jensen, B. A. Leita, K. S. Murray, B. Moubaraki, J. P. Smith, H. Toftlund, *Dalton Trans.* **2004**, 3370–3375.
[23] H. Köppen, E. W. Müller, C. P. Köhler, H. Spiering, E. Meissner, P. Gütlich, *Chem. Phys. Lett.* **1982**, *91*, 348–352.
[24] a) B. A. Katz, C. E. Strouse, *J. Am. Chem. Soc.* **1979**, *101*, 6214–6221; b) M. Mikami, M. Konno, Y. Saito, *Chem. Phys. Lett.* **1979**, *63*, 566–569; c) L. Wiehl, G. Kiel, C. P. Köhler, H. Spiering, P. Gütlich, *Inorg. Chem.* **1986**, *25*, 1565–1571.
[25] A. Hauser, J. Jeftic, H. Romstedt, R. Hinek, H. Spiering, *Coord. Chem. Rev.* **1999**, *190–192*, 471–491.
[26] D. Chernyshov, M. Hostettler, K. W. Törnroos, H.-B. Bürgi, *Angew. Chem.* **2003**, *115*, 3955–3960; *Angew. Chem. Int. Ed.* **2003**, *42*, 3825–3830; .
[27] a) V. Petrouleas, J. P. Tuchagues, *Chem. Phys. Lett.* **1987**, *137*, 21–25; b) D. Boinnarad, A. Bousseksou, A. Dworkin, J. M. Savariault, F. Varret, J. P. Tuchages, *Inorg. Chem.* **1994**, *33*, 271–281.
[28] A. B. Gaspar, V. Ksenofontov, J. A. Real, P. Gütlich, *Chem. Phys. Lett.* **2003**, *373*, 385–391.
[29] a) E. König, G. Ritter, S. K. Kulshreshtha, J. Waigel, L. Sacconi, *Inorg. Chem.* **1984**, *23*, 1241–1246; b) C. C. Wu, J. Jung, P. K. Gantzel, P. Gütlich, D. N. Hendrickson, *Inorg. Chem.* **1997**, *36*, 5339–5437.
[30] a) J. Fleisch, P. Gütlich, K. M. Hasselbach, W. Müller, *Inorg. Chem.* **1976**, *15*, 958–961; b) E. König, G. Ritter, S. K. Kulshreshtha, S. N. Nelson, *Inorg. Chem.* **1982**, *21*, 3022–3029; c) L. Wiehl, *Acta Crystallogr. B* **1993**, *49*, 289–297; d) G. S. Matouzenko, G. Molnar, N. Bréfuel, M. Perrin, A. Bousseksou, S. A. Borshch, *Chem. Mater.* **2003**, *15*, 550–556; e) G. S. Matouzenko, A. Bousseksou, S. A. Borshch, M. Perrin, S. Zein, L. Salmon, G. Molnar, S. Lecocq, *Inorg. Chem.* **2004**, *43*, 227–236.
[31] a) C. Le Vanda, K. Bechgaard, D. O. Cowan, M. D. Raush, *J. Am. Chem. Soc.* **1977**, *99*, 2964–2968; b) M. D. Ward, *Chem. Soc. Rev.* **1995**, *24*, 121–134; c) W. Skibar, H. Kopacka, K. Wurst, C. Salzmann, K. H. Ongania, F. Fabrizi de Biani, P. Zanello, B. Bildstein, *Organometallics* **2004**, *23*, 1024–1041.
[32] L. Duelund, R. Hazell, C. J. McKenzie, L. P. Nielsen, H. Toftlund, *J. Chem. Soc. Dalton Trans.* **2001**, 152–156.
[33] a) V. P. Dyakonov, G. G. Levchenko, *Sov. Sci. Rev. Sect. A Sov. J. Pribori Texnika Eksperimenta* **1983**, *5*, 236–242; b) M. Baran, G. G. Levchenko, V. P. Dyakonov, G. Shymchak, *Physica B+C* **1995**, *245*, 257–260.
[34] G. M. Sheldrick, SHELXS 97 and SHELXL 97. University of Göttingen (Germany), **1997**.
[35] J. Cosier and A. M. Glazer, *J. Appl. Crystallogr.* **1986**, *19*, 105–107.
[36] SMART-NT, Data Collection Software, Version 5.0; Bruker Analytical X-ray Instruments Inc., Madison, WI, USA, **1999**.
[37] SAINT-NT, Data Reduction Software, Version 5.0., Bruker Analytical Instruments Inc., Madison, Wisconsin, USA, **1999**.
[38] SHELXTL, Structure Refinement and Solution Software, Version 5.1., Bruker Anaytical Instruments Inc., Madison, Wisconsin, USA, **1999**.

Received: February 16, 2005
Published online: July 19, 2005

